Aerospace Science and Technology 111 (2021) 106574

Contents lists available at ScienceDirect

Aerospace Science and Technology

www.elsevier.com/locate/aescte

Infra-red line camera data-driven edge detector in UAV forest fire monitoring

Francesco De Vivo [a], Manuela Battipede [a,*], Eric Johnson [b]

[a] Polytechnic of Turin, Department of Mechanical and Aerospace Engineering, Corso Duca degli Abruzzi, 24, 10129 Torino, Italy
[b] Georgia Institute of Technology, School of Aerospace Engineering, 270 Ferst Drive, 30332-0150, Atlanta, GA, USA

ARTICLE INFO

Article history:
Received 14 July 2017
Received in revised form 29 January 2021
Accepted 10 February 2021
Available online 15 February 2021
Communicated by Tsourdos Antonios

Keywords:
Edge detection
Canny method
Contour algorithm
Forest fire
UAV
Infrared image

ABSTRACT

The accurate prediction of the wildfire spread-rate is a challenging task, due to the high number of parameters involved and the underlying complex dynamic multi-physics processes which drive the phenomenon. For these reasons, data-driven prediction tools could be useful to provide a more accurate prediction of the fire front. In this scenario, systematic fire data gathering becomes crucial and using an Unmanned Aircraft Vehicle (UAV) is strategic to reduce considerably the risk associated with flying a manned aircraft into low visibility and extremely turbulent air, sustained by the fire-induced convective motions.

Moreover the employment of the UAV is beneficial, as the possibility of flying at very low altitudes maximizes the on-board Electro-Optical (EO) sensor effectiveness. The aim is to develop a real time data-driven fire propagator to support wildfire fighting operations and to facilitate the risk assessment and decision making process. In order to collect data, the fire front position has to be measured using an infra-red (IR) camera so as to overcome the limitations associated to a visible camera in low visibility (smoky)conditions and night operations. To reduce the computational cost associated to the image processing, a Line Camera (LC) configuration has been preferred. Because of the mono-dimensionality of the measure, classical edge detector, like the Canny method, or contour algorithms, developed for 2D images, can not be applied. In this paper, a mono-dimensional noise-resistant algorithm for edge detection is presented. The generality of the proposed method opens the possibility to a variety of heterogeneous problems of different nature. The robustness of this algorithm resides in the use of known physical characteristics of the target of interest, to increase the feature edge discontinuity. Its straightforwardness guarantees fast computation, making it very attractive for real time image processing, remote sensing applications and for UAV surveillance tasks.

1. Introduction

Wildfire is a growing natural hazardous occurrence in most regions of Europe, United States and Australia, posing a threat to life and ecosystems [1]. This dramatically increasing trend is the consequence of the accumulation of flammable fuels, resulting from fire suppression, timber harvest, stock grazing and farm abandonment. Each year, wildfires are the main cause of destruction for more than 8 million acres of vegetation. These fires can be disastrous, as happened in June 2017, where raging forest fire in central Portugal killed more than 60 people, including at least 30 motorists who were trapped in their cars when the flames enveloped a stretch of road. Most large and intense fires have also the potential to injure or kill vulnerable fauna [2]. Fire effects on the landscape may be long-lasting and can produce secondary effects like erosion, changes in water quality, introduction of invasive species and produce landslides, that often are more catastrophic than the fire itself. For these reasons, the correct prediction of wildfire propagation is a key point in limiting damages and in supporting fire-fighters during operations.

Rothermel [3] developed a semi-empirical model that treats the front fire speed rate as a balance between the heat produced by the fire front and the heat absorbed by the fuel to reach the ignition temperature. This model builds upon the biomass fuel properties, the terrain orography and meteorological conditions, such as the wind speed at mid-flame height [4,5], the air tempera-

* Corresponding author.
E-mail addresses: francesco.devivo@polito.it (F. De Vivo), manuela.battipede@polito.it (M. Battipede), eric.johnson@ae.gatech.edu (E. Johnson).

https://doi.org/10.1016/j.ast.2021.106574
1270-9638/

Nomenclature

$\mathbf{I}(i,j)$	Image matrix	$\mathbf{I^o}(i,j)$	Subset of image intensity values
$\mathbf{K_n}$	Filtering kernel	I	Image pixel intensity
∇	Finite difference operator matrix	μ	Mean of the of the processed image
n_r, n_c	Number of pixels in rows and columns	σ	Standard deviation of the processed image
$\mathbf{I_s}(i,j)$	Filtered and derived image	I_b	Fireline intensity

Fig. 1. UAV in forest fire monitoring mission [1].

ture, the relative humidity and the presence of rain. Many research works have been dedicated to the improvement of the accuracy of these semi-empirical models and to their extension in order to get a more accurate solution [6–10]. Based on these models, several computer based fire simulators have been developed [11–15]. Unfortunately, the potential of these tools is limited by the large uncertainties associated to the accuracy of the physical models, as they do not take into account the interaction between the fire and the atmosphere. Moreover, they have a limited domain of validity, resulting from a calibration procedure based on laboratory experiments [16–18]. In order to overcome some of the current limitations, related to the semi-empirical models, the uncertainties in the input data need to be quantified and reduced. This task is achieved by monitoring the wildfire and using aerial images to improve the simulation results.

In 2009, NASA, in the framework of the Ikhana project [19], tested the potentials of delivering processed information to firefighters during a wildfire, by using a UAV equipped with Electro-Optical sensors Fig. 1. In 2012, Merino [20] showed how multiple UAVs can collaborate to automatically cover a wildfire area, in order to obtain a complete view of the fire extension. Yuan [21] conducted experiments to validate a method to extract and track fire pixels from UAV aerial video sequences. Pham [22] proposed a distributed control framework, designed for a team of UAVs that can closely monitor a wildfire in open space, and precisely track its development. McKenna [23] described the analysis of high spatial resolution UAV imagery, to assess fire severity by conducting experiments in Central Queensland, Australia. Recently, Lee [24] presented a wildfire detection system based on deep convolutional neural networks, employing UAVs to achieve high accuracy for a wide range of aerial photographs. Valero [25] introduced a system that processes aerial thermal infrared (TIR) images, in order to extract the parameters used to adjust a Rothermel-based simulator.

Image processing, in the majority of the cases, requires an on-board dedicated Computer Processing Unit (CPU), because of the computational cost associated to this task [26]. Moreover, if the data have to be processed off-line, high memory storage capabilities might be necessary. In case the data are sent to a ground control station, the bottleneck is located in the image compression and communication channel capabilities. In order to reduce the impact of the problem related to big data, a line camera configuration has been preferred. This configuration, very common in remote sensing [27], enables a 2D image to be built through a ground scanning, achieved thanks to the platform motion. This paper presents a process-while-scan algorithm to detect the forest fire edges. These data can be feed to a real-time non-linear filtering unit [28,29] to improve the fire propagator prediction. Several edge detector algorithms have been developed over the years. One of the most well established is the Canny method, which uses an optimal operator of the first derivative of the Gaussian function, to maximize the product of the signal-to-noise ratio for edge localization [30]. This approach is very effective in localizing edges, even if it is extremely sensitive to noise. A second drawback of this method is related to the choice of the fixed dual-threshold values to discriminate the feature edges. A wrong selection of these values might introduce errors in the solution, particularly in the case of complex background or very noisy images. For this reason, Othman [31,32] developed a modified version of the Canny

method, where the threshold values are automatically evaluated by using the solution proposed by Otsu [33]. Lindeberg proposed a method for automatic selection of the scale levels when detecting one-dimensional features, such as edges and ridges [34]. Asghari proposed a new computational approach for edge detection in biomedical application. This method transforms the image by emulating the propagation of light through a physical medium, with specific warped diffractive properties [35]. From the knowledge of the feature intensity level, a contour algorithm provides a solution similar to the one provided by an edge detector, with a lower level of false alarms. A presentation of the most recent algorithms for contour drawing can be found in [36]. Nevertheless, literature is populated by several algorithms for feature extraction and edge detection. Unfortunately none of these can be applied to a mono-dimensional image. For this reason, the authors developed a mono-dimensional process-while-scan algorithm for edge detection. This algorithm is very robust to noise, making the image pre-filtering unnecessary, while it is normally required in classical edge detection methods. This algorithm is very effective, because relies on a specific physical property of the observed features, to cancel out the image intensities related to the background or to undesired features. This physical property, in the case of a thermal camera, is the body temperature, that can be directly observed; otherwise it can be estimated on-line or known a-priori. To highlight the generality of this algorithm, it has also been applied to some medical images to delineate regions of pain and area of reduced blood flow due to the restriction of the artery.

2. Methodology

In this section the derivation of the proposed method is presented. As stated above, the method has been developed to process infrared line camera images, but it can be also applied to any 2D image, without restriction. The algorithm has been derived starting from the mathematical model of the Canny method. Given the image pixel matrix $\mathbf{I}(i,j)$, where $i = 1,\dots n_r$ and $j = 1,\dots n_c$ and where the pixel values, in a grey-scale image, are integers that range from 0 (black) to 255 (white), the first step of the Canny method is to filter $\mathbf{I}(i,j)$, using a Gaussian kernel $\mathbf{K_n}$, where the subscript $\mathbf{n}$ in the kernel indicates its dimension. The values n_r and n_c are respectively the number of image pixels along rows and columns. Once the image has been filtered, the Canny method proceeds by calculating the gradient of the resulting image, by applying a first order difference approximation. To indicate the finite difference matrix, the symbol ∇ is used. Because the filtering and the derivative operators are linear, they can be applied in any order. By applying the smoothing and derivative operator, the resulting image $\mathbf{I_s}(i,j)$ is

$$\mathbf{I_s}(i,j) = \mathbf{K_n}\nabla * \mathbf{I}(i,j) \tag{1}$$

where the symbol $*$ is the convolution operator. In the proposed algorithm, the image is a mono-dimensional array, so the second index j can be dropped and the matrices $\mathbf{K_n}$ and ∇ reduce to vectors. Assuming that the object in the image, for which the edges have to be determined, has an observable physical parameter that can assume values in the interval $[T_{min}, T_{max}]$, an intensity subset $\mathbf{I^o}$ can be defined as follows

$$\mathbf{I^o} \subseteq \mathbf{I} \quad | \quad I_{min} \leq I^o \leq I_{max} \tag{2}$$

where $[I_{min}, I_{max}]$ are the pixel intensity values associated to $[T_{min}, T_{max}]$. If the pixel intensity $I(i)$ of the image is outside the interval $[I_{min}, I_{max}]$, the intensity value of this pixel is set to 0

$$\forall i \in [1, n_r] \quad \text{if} \quad \mathbf{I}(i) \not\subseteq \mathbf{I^o} \Rightarrow \mathbf{I}(i) = 0. \tag{3}$$

This artifice makes the absolute value of the derivative $\mathbf{I_s}$ rise to very high values in correspondence of the edges. This process makes the algorithm very robust to image noise, avoiding the problem of false edge detection, which is common in the Canny method. The second advantage of having a high signal-to-noise ratio is to make the filtering unnecessary, simplifying the Equation (1) as follows

$$\mathbf{I_s}(i) = \nabla * \mathbf{I}(i). \tag{4}$$

The next step is to define a threshold δ to classify the points belonging to the edge. In order to overcome the limitations related to the fixed threshold values of the Canny method, a solution implementing a dynamic threshold has been adopted. Considering that the edges, in the processed image, are points for which there is a high discontinuity of the intensity values, they can be seen as spikes of the derivative. Calculating the standard deviation of the vector $\mathbf{I_s}$, the threshold value can be set to three times the standard deviation $\delta = 3\sigma$. In order to speed-up the process, the standard deviation is calculated using a recurrence formula. A numerically stable solution to calculate σ has been proposed by Knuth [37]. In this algorithm, the quadratic deviation value of the pixel intensity Σ is initialized to 0 and the sampled mean value is set to $\mu = \mathbf{I_s}(1)$. After the initialization, the following recurrence formulas are used to calculate the generic $\mathbf{I_s}(i)$

$$\begin{cases} \mu_i &= \mu_{i-1} + \frac{\mathbf{I_s}(i) - \mu_{i-1}}{i} \\ \Sigma_i &= \Sigma_{i-1} + [\mathbf{I_s}(i) - \mu_{i-1}][\mathbf{I_s}(i) - \mu_i] \end{cases} \tag{5}$$

for $i = 2\dots n_r$. When the entire vector has been processed, the value of σ can be calculated as

$$\sigma = \sqrt{\frac{\Sigma}{n_r - 1}}. \tag{6}$$

In Equation (4), the derivative operator ∇ is defined as follows

$$\nabla = \frac{1}{2}\begin{bmatrix} -1 & 0 & 1 \end{bmatrix}, \tag{7}$$

but, considering that the threshold value is dynamically calculated and depends on the value assumed by σ, the multiplicative term $1/2$ becomes only a scale factor that does not affect the solution. For this reason, it can be neglected. This simplification avoids the calculation of an expensive division at each step, and reduces Equation (4) to a simple subtraction of the intensity values

$$\mathbf{I_s}(i) = \mathbf{I}(i+1) - \mathbf{I}(i-1). \tag{8}$$

Once the vector processing is completed, the edge pixels can be identified as follows

$$\text{if} \quad \mathbf{I_s}(i) > 3\sigma \wedge \mathbf{I}(i) > 0 \Rightarrow \mathbf{I}(i) = \text{edge point}. \tag{9}$$

In Table 1 the algorithm implementation is summarized.

3. Results

This section presents the numerical results of the algorithm, applied to different images to investigate on its advantages and shortcomings. The algorithm has been validated by comparing the solution with the one provided by the Canny method and the contour algorithm. The results proposed in this paper have been obtained using MATLAB as the software environment on an Intel Core i7-4710HQ 64 bit, 2.50 GHz with 16 GB RAM. In order to

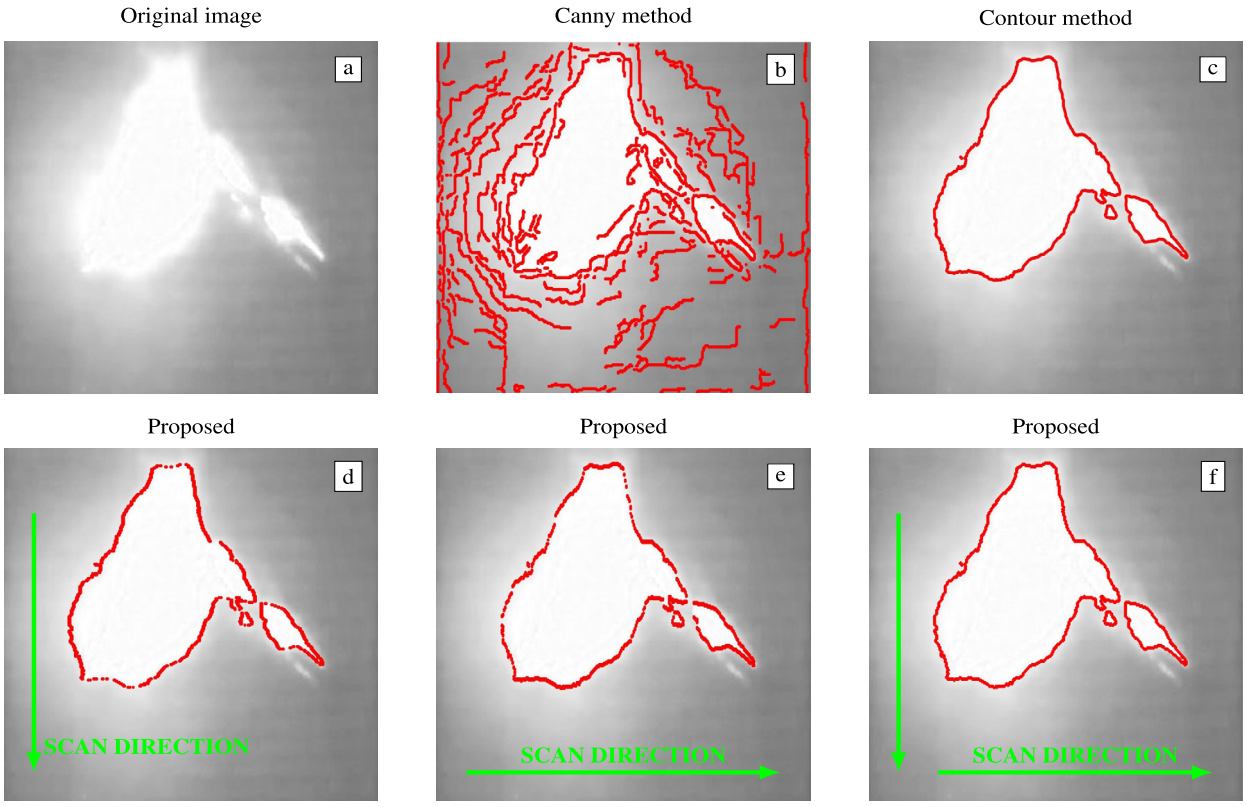

Fig. 2. Comparison of the proposed method with the solution provided by the contour algorithm and the Canny method. The results of the proposed method are shown for row-aligned scan direction, column-aligned scan direction and for both scan directions.

Table 1
Edge detection algorithm.

Initialize $\mu = 0$ and $\Sigma = 0$

for each image pixel **do**

if $I_{min} \lneq \mathbf{I}(i-1) \lneq I_{max} \Rightarrow \mathbf{I}(i-1) = 0$

if $I_{min} \lneq \mathbf{I}(i+1) \lneq I_{max} \Rightarrow \mathbf{I}(i+1) = 0$

calculate $\mathbf{I_s}(i) = \mathbf{I}(i+1) - \mathbf{I}(i-1)$

$$\mu_i = \mu_{i-1} + \frac{\mathbf{I_s}(i) - \mu_{i-1}}{i}$$

$$\Sigma_i = \Sigma_{i-1} + [\mathbf{I_s}(i) - \mu_{i-1}][\mathbf{I_s}(i) - \mu_i]$$

end

calculate the standard deviation $\sigma = \sqrt{\frac{\Sigma}{n_r - 1}}$

find the edge points with $\mathbf{I_s}(i) > 3\sigma \wedge \mathbf{I}(i) > 0$

apply the algorithm, it is sufficient to know the value of the measurable physical parameter associated to the feature that has to be extracted. In case the image depicts a forest fire and no temperature reference is available, a realistic temperature range can be estimated from a mathematical model which estimates the fireline intensity I_b. According to the Stefan Boltzman irradiation law, this intensity is proportional to the fourth power of the temperature. The fire intensity, in kW/m, can be approximatively calculated by using the model proposed by Byram [38]

$$I_b = \frac{I_R}{60}\frac{12.6R}{\sigma_f} \tag{10}$$

where I_R is the reaction intensity in kJ/min/m^2 and σ_f is the characteristic surface area-to-volume ratio of the fuel bed in m^{-1}. R in Equation (10) is the Rothermel fire spread rate in m/min, calculated as follows

$$R = \frac{I_R \zeta (1 + \Phi_s + \Phi_w)}{\rho_b \epsilon Q_{ig}} \tag{11}$$

where the numerator represents the heat source, whereas the denominator is the heat sink. I_R has been defined in Equation (10), whereas ζ is the no-wind propagating flux ratio. Φ_s and Φ_w are respectively the slope and wind correction factors, ρ_b is the bulk density in kg/m^3, ϵ is the effective heating number and Q_{ig} is the heat of pre-ignition in kJ/kg. The complete algorithm to calculate each of these coefficients is described in [3]. The fireline intensity, calculated using Equation (10), can be used as an initialization value for a more accurate parameter estimation filtering process. Once the expected value μ_p and an accuracy σ_p are obtained from the filtering step, the boundaries are calculated as follows

$$\begin{bmatrix} T_{min} \\ T_{max} \end{bmatrix} = \begin{bmatrix} \mu_p - k\sigma_p \\ \mu_p + k\sigma_p \end{bmatrix} \tag{12}$$

where k is an arbitrary coefficient, chosen to set the width of the interval in terms of standard deviation. After the temperature interval, which better represents the fire temperature environment, has been calculated, a quantization process is performed to convert the physical temperature values in image pixel intensity. In Fig. 2.a, an infrared image of a hot spot is analyzed. This image, characterized by smooth edges of the region of interest, has been selected to highlight the robustness of the proposed approach with respect to the Canny method, affected by false edge detection. Fig. 2.b shows the result of the Canny method applied to the original image, whereas in Fig. 2.c the result obtained by applying the contour algorithm is presented. The intensity interval used in the proposed algorithm is [230, 255], selected through a trial and error procedure to better represent the fireline. The value used in the contour method is the mean value in this interval. This choice is driven by the necessity of comparing the algorithm results by using the same

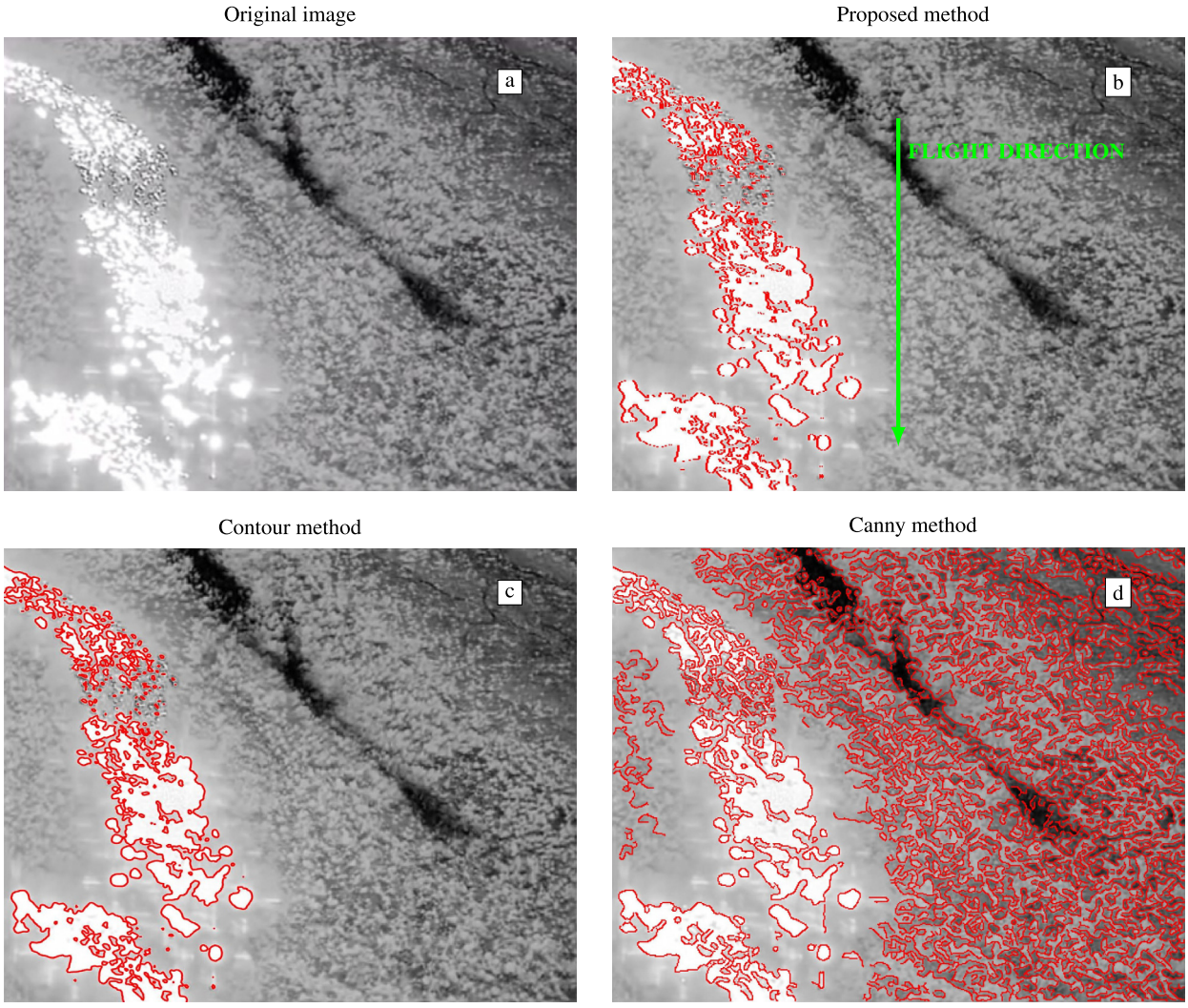

Fig. 3. Comparison of the proposed method with the solution provided by the contour algorithm and the Canny method. In the proposed method the scan direction is indicated by the green arrow. The image is relative to a forest fire 20 miles south-west of Meeker, CO [39]. (For interpretation of the colors in the figure(s), the reader is referred to the web version of this article.)

input conditions. By comparing the Fig. 2.b and Fig. 2.c, it is clear that, for this kind of application, the contour algorithm outperforms the Canny method, which detects a very relevant number of false edges. In the second raw of images of Fig. 2, three solutions of the proposed algorithm are presented. Fig. 2.d shows the solution relative to a vertical scan direction. In this condition, the image is acquired and processed row-by-row, which means that also the gradient is calculated row-wise. In this case, when the maximum image gradient direction is in the scan direction (vertical) some contour points remain undetected. Fig. 2.e shows the solution obtained by processing the image column-by-column. As expected, also in this case some contour points are lost in the perpendicular direction, for the same reason anticipated for Fig. 2.d. In Fig. 2.f, the image is processed along both rows and columns. In this case, the solution is perfectly coincident with the one provided by the contour method without any point loss. Comparison with the Contur method has both validated the proposed algorithm and proven the higher performance of the algorithm with respect to the Canny method. The zeroing process, performed on pixels with intensity values outside the prescribed boundaries, has impressively reduced the noise effect on the result, reducing the possibility of mistakenly detecting false edges, as for the Canny method. The irrelevant number of points not detected along the edges, when the image is scanned along a single dimension, confirms the validity of the assumption to use a 1D derivative operator instead of a more computationally expensive Sobel or Prewitt operators [40]. This important result allows us to use this monodimensional and computationally inexpensive $\mathcal{O}(N)$ algorithm for processing images generated using a line camera, without loss of accuracy.

Fig. 3 represents an infrared image, taken with a UAV, related to a forest fire located 20 miles south-west of Meeker, Colorado [39]. Fig. 3.a shows the original image, whereas the solution obtained by applying the proposed algorithm is presented in Fig. 3.b. As indicated by the green arrow, the flight direction of the platform has been assumed to be parallel to the fire front, whereas the camera footprint is orthogonal to this direction. With this configuration, the image is scanned row-by-row. The solution is compared with the one obtained by applying the contour algorithm in Fig. 3.c and the Canny method in Fig. 3.d. As previously observed, the solution of the Canny method is completely unacceptable for our application. Also in this case, the accuracy obtained by the proposed algorithm is comparable with the one obtained by using the contour method.

In the case of Fig. 4, the proposed algorithm has been applied to the infrared image of a burning surface [39]. The complexity of the image emphasizes the capability of the algorithm of processing any shape. The image on the right of Fig. 4 shows the value of the threshold σ, calculated by applying the algorithm of Table 1

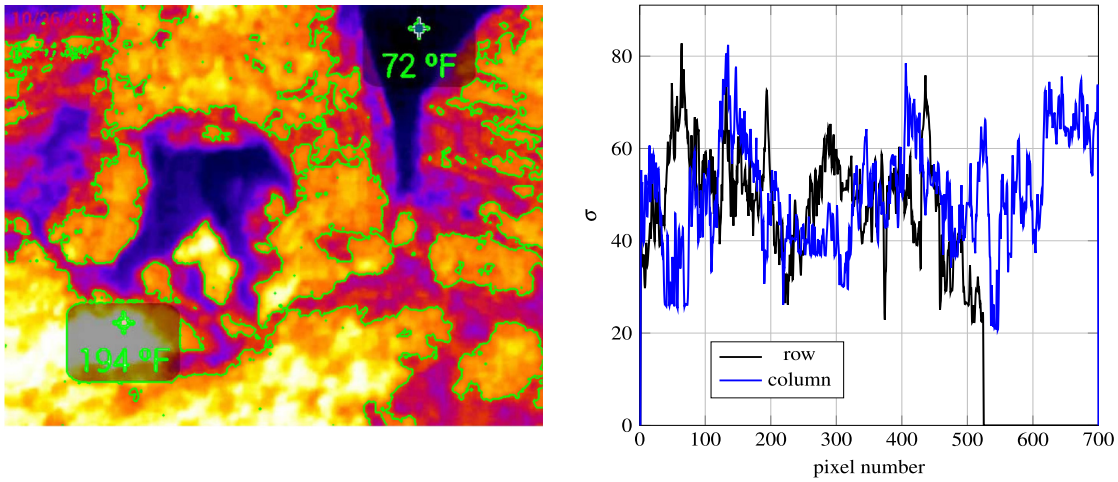

Fig. 4. In the left image [39], the solution provided by the proposed algorithm is highlighted in green, whereas in the right figure the value of the standard deviation σ is shown for each image row and column.

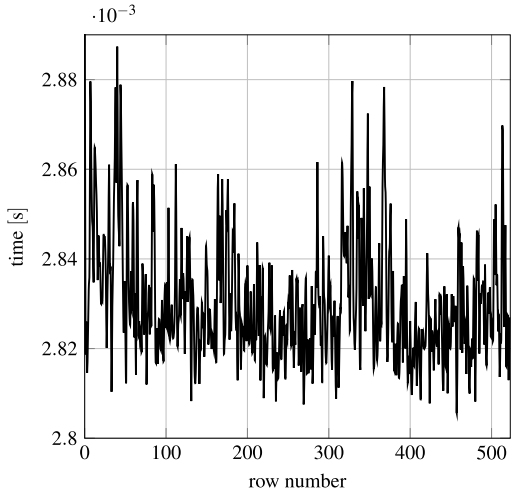

Fig. 5. Simulation time necessary to process each row of the left image of Fig. 4. The row dimension is of 700 pixels. The result is relative to the average of 100 runs.

row-wise (black line) and column-wise (blue line). In both cases, observing the high variability of σ it is clear that the local σ value cannot be used for the proximity rows (or columns). The accuracy of the solution can be guaranteed only by using a dynamic threshold, calculated for each row (or column).

Fig. 5 shows the simulation time required to process each row of the image of Fig. 4. The number of pixels per row is 700. In order to reduce the noise in the time measurement, the solution has been averaged over 100 runs. The computational time of the MATLAB simulation is in the order of 10^{-3} s, which meets the time specification imposed by a real time application.

4. Technology transfer

In order to demonstrate the generality of the proposed approach, the algorithm has been applied to two infrared medical images. Fig. 6.a shows the case of a chronic pain: local pain in the area of the injury is generally seen to be hyperthermic, with an increase of thermal emissions, whereas areas of referred pain are generally seen to be hypothermic. These two different areas are perfectly outlined by the algorithm, as shown in Fig. 6.b. A different situation is presented in Fig. 6.c, where the thermal image shows the areas of blood flow when there is an artery restriction. Also in this case, the colder region is well outlined by the algorithm, as shown in Fig. 6.d. The two additional cold regions identified by the algorithm could be filtered out in a simple way by including an additional information about the body anatomy.

5. Conclusions

In this paper, a very straightforward and computationally efficient edge detection algorithm is presented. The algorithm has been developed to overcome the shortcomings of existent and well established contour and edge detection algorithms, applied to a line camera image. The necessity of using a line scan camera and to develop a dedicated algorithm, arises from the requirement to sequentially provide a measure of the fire front to a data-drive fire simulator. The proposed edge detection algorithm takes advantage of the physical characteristics of the observed feature, to increase the signal-to-noise ratio, whereas the variable threshold allows the compensation of the image intensity variation. The solution has been compared to two conceptually different edge detection algorithms: the Canny and the contour methods. From the simulation results, the solution provided by the proposed method is validated by the contour algorithm, and the performance are higher than the Canny method, which is affected by a high rate of false alarms. The time required by the algorithm to process a 700 pixel vector also opens the possibility of implementation in real time applications. The algorithm, for its straightforwardness and generality, can process any kind of thermal image, widening the spectrum of applications in which it can be used. To confirm this point, two medical images, relative to two different kinds of diseases, have been successfully processed.

Declaration of competing interest

The authors declare that there are no conflicts of interest.

References

[1] E. Cheng, Drones podrían detectar incendios forestales automáticamente, visited on 20/06/2017, http://www.emol.com/noticias/Tecnologia/2016/10/26/828436/Drones, 2016.
[2] L.J. Lyon, M.H. Huff, R.G. Hooper, E.S. Telfer, D.S. Schreiner, J.K. Smith, Wildland Fire in Ecosystems Effects of Fire on Fauna, USDA, 2000, http://digitalcommons.unl.edu/cgi/viewcontent.cgi?article=1006&context=jfspsynthesis.
[3] R.C. Rothermel, A Mathematical Model for Predicting Fire Spread in Wildland Fuels, USDA Forest Service, 1972.
[4] P.L. Andrews, Modeling wind adjustment factor and midflame wind speed for Rothermel's surface fire spread model, Tech. rep., Rocky Mountain Research Station, 2012.

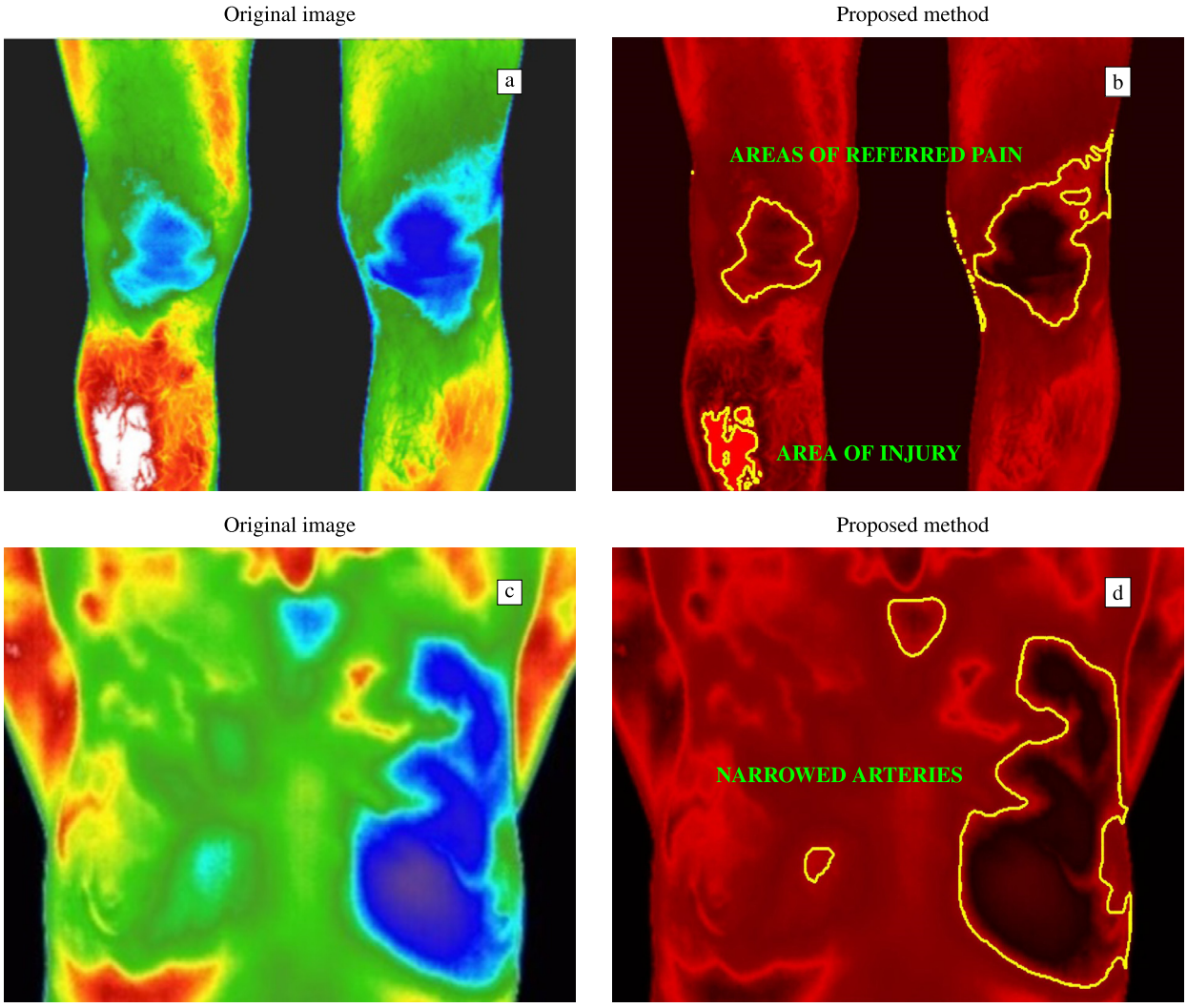

Fig. 6. Proposed edge detector algorithm in medical images [41] application.

[5] W.J. Massman, J. Forthofer, M.A. Finney, An improved canopy wind model for predicting wind adjustment factors and wildland fire behavior, Can. J. For. Res. 47 (999) (2017) 594–603.
[6] F.A. Albini, I. Forest, et al., Computer based models of wildland fire behavior, in: Intermountain Forest and Range Experiment Station, Forest Service, US Department of Agriculture, 1976.
[7] R.C. Rothermel, Predicting behavior and size of crown fires in the northern rocky mountains, Tech. rep., US Department of Agriculture, Forest Service, Rocky Mountain Research Station Ogden, UT, 1991.
[8] D. Prince, C. Shen, T. Fletcher, Semi-empirical model for fire spread in shrubs with spatially-defined fuel elements and flames, Fire Technol. (2017) 1–31.
[9] J.H. Scott, E.D. Reinhardt, Assessing crown fire potential by linking models of surface and crown fire behavior, Tech. rep., Rocky Mountain Research Station, 2001.
[10] M.E. Alexander, M.G. Cruz, Corrigendum to: interdependencies between flame length and fireline intensity in predicting crown fire initiation and crown scorch height, Int. J. Wildland Fire 26 (4) (2017) 345.
[11] J.M. Forthofer, B.W. Butler, C.W. McHugh, M.A. Finney, L.S. Bradshaw, R.D. Stratton, K.S. Shannon, N.S. Wagenbrenner, A comparison of three approaches for simulating fine-scale surface winds in support of wildland fire management. Part II. An exploratory study of the effect of simulated winds on fire growth simulations, Int. J. Wildland Fire 23 (7) (2014) 982–994.
[12] K. Kalabokidis, P. Palaiologou, M.A. Finney, Fire behavior simulation in Mediterranean forests using the minimum travel time algorithm, in: Looking Toward the Future in a Changing Environment, 2014, pp. 468–492.
[13] J.-B. Filippi, X. Pialat, C.B. Clements, Assessment of ForeFire/Meso-NH for wildland fire/atmosphere coupled simulation of the FireFlux experiment, Proc. Combust. Inst. 34 (2) (2013) 2633–2640.
[14] C. Tymstra, R. Bryce, B. Wotton, S. Taylor, O. Armitage, et al., Development and structure of Prometheus: the Canadian wildland fire growth simulation model, Information Report NOR-X-417, Natural Resources Canada, Canadian Forest Service, Northern Forestry Centre, Edmonton, AB, 2010.
[15] D. Chong, K. Tolhurst, T. Duff, Phoenix Rapidfire 4.0's Convection and Ember Dispersal Model, Bushfire CRC, 2012.
[16] D. Viegas, Overview of forest fire propagation research, Fire Saf. Sci. 10 (2011) 95–108.
[17] M.G. Cruz, M.E. Alexander, Uncertainty associated with model predictions of surface and crown fire rates of spread, Environ. Model. Softw. 47 (2013) 16–28.
[18] M.A. Finney, J.D. Cohen, S.S. McAllister, W.M. Jolly, On the need for a theory of wildland fire spread, Int. J. Wildland Fire 22 (1) (2013) 25–36.
[19] P.W. Merlin, Ikhana: Unmanned Aircraft System Western States Fire Missions, National Aeronautics and Space Administration, NASA History Office, 2009.
[20] L. Merino, F. Caballero, J.R. Martínez-de Dios, I. Maza, A. Ollero, An unmanned aircraft system for automatic forest fire monitoring and measurement, J. Intell. Robot. Syst. 65 (1) (2012) 533–548, https://doi.org/10.1007/s10846-011-9560-x.
[21] C. Yuan, Z. Liu, Y. Zhang, Aerial images-based forest fire detection for firefighting using optical remote sensing techniques and unmanned aerial vehicles, J. Intell. Robot. Syst. (2017) 1–20, https://doi.org/10.1007/s10846-016-0464-7.
[22] H.X. Pham, H.M. La, D. Feil-Seifer, M. Deans, A distributed control framework for a team of unmanned aerial vehicles for dynamic wildfire tracking, CoRR, arXiv:1704.02630, 2017.
[23] P. McKenna, P.D. Erskine, A.M. Lechner, S. Phinn, Measuring fire severity using UAV imagery in semi-arid central Queensland, Australia, Int. J. Remote Sens. 38 (14) (2017) 4244–4264, https://doi.org/10.1080/01431161.2017.1317942.
[24] W. Lee, S. Kim, Y.T. Lee, H.W. Lee, M. Choi, Deep neural networks for wild fire detection with unmanned aerial vehicle, in: 2017 IEEE International Conference on Consumer Electronics (ICCE), 2017, pp. 252–253.
[25] M.M. Valero, O. Rios, C. Mata, E. Pastor, E. Planas, An integrated approach for tactical monitoring and data-driven spread forecasting of wildfires, Fire Saf. J. (2017), https://doi.org/10.1016/j.firesaf.2017.03.085.

[26] F.D. Vivo, M. Battipede, P. Gili, Occlusion points identification algorithm, Comput. Aided Des. 91 (2017) 75–83, https://doi.org/10.1016/j.cad.2017.06.005, http://www.sciencedirect.com/science/article/pii/S0010448517301185.
[27] H. Yu, Q. Wang, Z. Zhang, Z.-j. Zhang, W. Tang, X. Tang, S. Yue, C.-s. Wang, Oil spill detection using hyperspectral infrared camera, in: Infrared, Millimeter-Wave, and Terahertz Technologies IV, vol. 10030, 2017, 100301G.
[28] F. De Vivo, A. Brandl, M. Battipede, P. Gili, Joseph covariance formula adaptation to Square-Root Sigma-Point Kalman filters, Nonlinear Dyn. 88 (3) (2017) 1969–1986, https://doi.org/10.1007/s11071-017-3356-x.
[29] F. De Vivo, M. Battipede, P. Gili, A. Brandl, Ill-conditioned problems improvement adapting Joseph covariance formula to non-linear Bayesian filters, WSEAS Trans. Electron. 7 (2016) 18–25.
[30] J. Canny, A computational approach to edge detection, IEEE Trans. Pattern Anal. Mach. Intell. PAMI-8 (6) (1986) 679–698.
[31] Z. Othman, A. Abdullah, An adaptive threshold based on multiple resolution levels for Canny edge detection, in: Recent Trends in Information and Communication Technology: Proceedings of the 2nd International Conference of Reliable Information and Communication Technology (IRICT 2017), Springer International Publishing, Cham, 2018, pp. 316–323.
[32] Z. Othman, A. Abdullah, A.S. Prabuwono, A statistical approach of multiple resolution levels for canny edge detection, in: 2012 12th International Conference on Intelligent Systems Design and Applications (ISDA), 2012, pp. 837–841.
[33] N. Otsu, A threshold selection method from gray-level histograms, IEEE Trans. Syst. Man Cybern. 9 (1) (1979) 62–66.
[34] T. Lindeberg, Edge detection and ridge detection with automatic scale selection, in: Proceedings CVPR IEEE Computer Society Conference on Computer Vision and Pattern Recognition, 1996, pp. 465–470.
[35] M.H. Asghari, B. Jalali, Edge detection in digital images using dispersive phase stretch transform, Int. J. Biomed. Imaging 2015 (2015) 6, https://doi.org/10.1155/2015/687819.
[36] J. Seo, S. Chae, J. Shim, D. Kim, C. Cheong, T.-D. Han, Fast contour-tracing algorithm based on a pixel-following method for image sensors, Sensors 16 (3) (2016) 353, https://doi.org/10.3390/s16030353.
[37] D.E. Knuth, The Art of Computer Programming: Sorting and Searching, Vol. 3, Pearson Education, 1998.
[38] R. Wilson, Reformulation of Forest Fire Spread Equations in SI Units, vol. 292, Dept. of Agriculture, Forest Service, Intermountain Forest and Range Experiment Station, 1980.
[39] B. Gabbert, Fire aviation, visited on 20/06/2017, http://fireaviation.com/, 2017.
[40] R. Jain, R. Kasturi, B.G. Schunck, Machine Vision, vol. 5, McGraw-Hill, New York, 1995.
[41] Thermal eyez, visited on 20/06/2017, https://www.thermaleyez.com/full-body-or-selected-area-scan/.